Pre-print version of: Koulali, A., Radomski, P., De Sio, L., Mikielewicz, D., & Ziółkowski, P. (2024). CFD COUPLING OF VOF MODEL WITH ARRHENIUS EQUATION FOR ANALYSIS OF LASER-INDUCED THERMAL DEACTIVATION OF E. COLI. https://doi.org/10.1615/tfec2024.sim.051258

ASTFE
American Society
of Thermal and Fluids Engineers

9th Thermal and Fluids Engineering Conference (TFEC)
April, 21-24, 2024
Partially Online Virtual and at Oregon State University, OR

TFEC-2024-xxxxx

CFD COUPLING OF VOF MODEL WITH ARRHENIUS EQUATION FOR ANALYSIS OF LASER-INDUCED THERMAL DEACTIVATION OF E. COLI

A. Koulali,[1,*] P. Radomski,[1] L. De Sio,[2] D. Mikielewicz,[1] P. Ziółkowski[1]

[1]Gdańsk University of Technology, Faculty of Mechanical Engineering and Ship Technology, Poland
[2]Department of Medico-Surgical Sciences and Biotechnologies Sapienza University of Rome, Latina, Italy

ABSTRACT

Understanding bacterial deactivation at the micro-scale, particularly with E. coli, is crucial for advancing microbiology and has promising applications in biomedical research. In this research contribution, we investigate the thermal inactivation of E. coli bacteria through the use of gold nanoparticles irradiated by a laser within a microfluidic chamber. The microfluidic device comprises a fluidic chamber filled with a thin film of water and air (1 mm thick). The chamber is constructed with 1 mm PDMS coating on the top and side walls, and 1 mm Borosilicate glass on the bottom. Computational Fluid Dynamics (CFD) calculations are executed using ANSYS Fluent software employing the Volume of Fluid (VOF) multi-phase model. Bacterial deactivation is described by a first-order kinetic model, while the Arrhenius equation is employed to define the decay coefficient. The light-heat conversion is modeled using a literature-based approach, validated against experimental data. Our findings affirm the efficacy of the proposed physical model (laser + gold nanoparticles) for bacterial inactivation. Additionally, we propose an innovative approach by integrating bacterial inactivation equations with the VOF model, opening avenues for further applications in the field.

KEY WORDS: Microfluidic, Laser-Induced Heating, Gold Nanoparticles, E. coli Deactivation, Computational Simulation, Arrhenius equation, VOF model

1. INTRODUCTION

Bacterial inactivation is an essential, multi-faceted field with applications in a variety of areas, including healthcare, food safety and environmental protection. Scientists have addressed their challenge to remove pathogenic bacteria using a variety of approaches including heat, chemicals and radiation [1]. Heat treatment is a commonly used disinfection method, particularly in environments where resources are limited. It relies on the combined factors of temperature and exposure time to reduce the presence of various groups of pathogens, such as bacteria, viruses and microbes [2]. Among these, laser-induced heat treatment with gold nanoparticles is a significant breakthrough [3–7]. The precision of laser irradiation permits targeted heating, while gold nanoparticles enhance the heat-generating process [4, 5]. This combined approach offers advantages in terms of specificity and efficiency in bacterial inactivation. The controlled application of laser beams, facilitated by gold nanoparticles, represents a promising avenue for improved and customized bacterial treatment strategies across various domains.

Recent developments in the field, however, have given rise to a new perspective. The integration of Computational Fluid Dynamics (CFD) into bacterial inactivation studies has sparked a paradigm shift. CFD allows for a more comprehensive understanding of fluid dynamics and heat transfer, offering the ability to simulate

*Corresponding A. Koulali: aimad.koulali@pg.edu.pl

and experiment with varying parameters that are often difficult to control in traditional laboratory settings. Early studies relied mainly on empirical observations [8, 9], but recent studies have adopted CFD to unravel the intricacies of fluid dynamics and heat transfer in biosystems [10–12]. This evolution offers researchers the ability to simulate diverse scenarios and fine-tune variables that are difficult to control in conventional experimental set-ups. The intersection of experimental breakthroughs and computational modelling has not only broadened our understanding of bacterial inactivation mechanisms, but has also paved the way for more sophisticated and personalized treatment strategies. As we delve deeper into the intricacies of our study, it becomes clear that this confluence of experimental and computational approaches holds tremendous promise for advancing the field of bacterial inactivation.

Amidst these advancements, modelling light-to-heat conversion by gold nanoparticles is a challenge [13, 14]. Recent models treat the interaction indirectly as boundary condition with heat generation, simplifying thermodynamic investigations but neglecting the explicit laser beam presence [5, 13, 14]. Challenges arise in accurately modelling dispersed nanoparticles, considering nanoscale distances and dependence on nanostructure [13]. Despite these complexities, this modelling approach aligns with our focus on thermodynamics, especially when a detailed laser beam profile is not the primary concern.

The other complicated aspect of integrating CFD into bacterial inactivation studies is describing the behaviour of bacteria in the face of temperature changes, i.e. quantifying the number of bacterial cells inactivated during the process. For bacterial inactivation studies, researchers often use the simplicity and efficiency of the first-order kinetic model to describe the cell deactivation process [9, 11, 12, 15].This model assumes that the rate of bacterial inactivation is directly proportional to the number of active cells present, with a constant rate of decay. This model provides a practical framework for understanding bacterial deactivation kinetics, allowing researchers to quantify the reduction in the number of viable cells over time [16]. The first-order kinetic model has found widespread application due to its simplicity and empirical accuracy, offering valuable insights into the dynamics of bacterial inactivation. Additionally, the Arrhenius equation plays a pivotal role in elucidating the temperature dependence of bacterial decay rates. The Arrhenius equation provides a quantitative link between temperature and the rate of bacterial inactivation [17–19]. It highlights the sensitivity of bacterial kinetics to temperature variations, offering crucial insights for optimizing thermal treatment strategies. By incorporating these mathematical models into the Computational Fluid Dynamics (CFD) framework, we can simulate and predict the intricate dynamics of bacterial inactivation under varying conditions, contributing to the advancement of tailored and effective treatment strategies.

Within the framework of our physical model, featuring a stable interface with a static configuration of a thin film of water containing bacteria, it is relevant to introduce numerical methods commonly employed in addressing scenarios with persistent fluid interfaces. Various computational approaches have been developed to simulate the dynamics of two-phase flows (see [20]), even when the interface remains stationary. Examples of such methods include the Level Set Method (LSM), the Front-Tracking Method, and the Phase Field Method, all designed to accurately represent complex interactions within multi-phase systems, particularly those involving thin liquid films. Among these approaches, the Volume of Fluid (VOF) method emerges as a widely adopted and versatile choice, even in scenarios where the interface doesn't undergo significant changes. The VOF method excels in handling multi-phase flows by tracking the volume fractions of different fluids within each computational cell, providing an accurate representation of the coexistence of air and a thin film of water. The study conducted by [21] evaluates the accuracy of the Volume-of-Fluid (VOF) model integrated into FLUENTTM, confirming its effectiveness in representing thin liquid film flows in rectangular cavities with accurate surface profiles, particularly under low or zero surface tension conditions, while recognizing limitations in handling high surface tension values. Its applicability extends across various domains, including microfluidic, where the presence of distinct phases is crucial to understanding system behavior (see [22]). In addition, [23] demonstrates that the application of the VOF model substantiates its suitability for investigating thin films, affirming its effectiveness in the realm of tear film dynamics. Despite the static nature of the interface in our study, the VOF method proves invaluable in accurately capturing the coexistence of air and the thin film of water. Its implementation ensures a robust representation of the two-phase system, enabling a comprehensive analysis of thermal interactions within the microfluidic chamber.

2. MOTIVATION

In the field of bacterial inactivation, where the challenge of designing effective and precise methods is always present, our study finds its motivation in the convergence of advanced techniques within a microfluidic environment. The integration of gold nanoparticles, laser-induced heat treatment and computational fluid dynamics (CFD) opens up a new era of exploration, promising advances with wide-ranging implications for healthcare, food safety and environmental protection. The motivation to study the thermal inactivation of E. coli in this microfluidic chamber comes from the complexities associated to this controlled system. Featuring a borosilicate glass base and PDMS lid, the cylindrical chamber encapsulates an experimental environment in which gold nanoparticles, precisely placed at the bottom of the chamber, respond to laser irradiation, converting light into heat provides an ideal means of precisely inactivating bacteria. Our research is motivated not only by the search for the fundamental mechanisms of bacterial inactivation, but also by the need to go beyond the limits of empirical observations.

3. KEY COMPONENTS OF THE SIMULATION:

3.1 Device description:

The cylindrical microfluidic chamber consists of a borosilicate glass base (1 mm thick) coated with a layer of PDMS. The 2 mm-thick microfluidic chamber contains air and a thin film of water (100 μm) hosting E.coli bacteria. The bottom of the chamber is embedded with gold nanoparticles see Fig. 1.

3.2 Standard Governing Equations:

3.2.1 VOF Model : The Volume of Fluid (VOF) model is adopted to accurately represent the presence of two phases (water and air) within the microchamber. Interface dynamics are represented by the following conservation equation [23, 24]:

$$\frac{\partial \alpha}{\partial t} + u \cdot \nabla \alpha = 0 \tag{1}$$

The volume fraction field α takes the values:

- $\alpha = 0$: in the air phase.
- $\alpha = 1$: in the thin water film.
- $0 < \alpha < 1$: indicates the presence of the two phases separated by an interface.

In an unsteady state, within a laminar regime in a 3D flow [25], taking into account the presence of bacteria in a thin film of water, all thermal properties are treated as effective. Indeed, they are calculated simultaneously, integrating the thermal characteristics of both water and bacteria.

- Fluid region
  Continuity equation

$$\frac{\partial \rho_{\text{eff}}}{\partial t} + \nabla \cdot (\rho_{\text{eff}} \vec{v}) = 0 \tag{2}$$

  Momentum equation

$$\frac{\partial (\rho_{\text{eff}} \vec{v})}{\partial t} + \nabla \cdot (\rho_{\text{eff}} \vec{v}) = -\nabla p + (\mu_{\text{eff}} [(\nabla \vec{v} + \nabla \vec{v}^{\text{tr}}) - \frac{2}{3} \nabla \cdot \vec{v} I]) + \rho_{\text{eff}} \vec{g} \tag{3}$$

  Energy equation

$$\frac{\partial (\rho_{\text{eff}} C p_{\text{eff}} T_{\text{f}})}{\partial t} + \nabla \cdot (\vec{v} (\rho_{\text{eff}} C p_{\text{eff}} T_{\text{f}})) = \nabla \cdot (k_{\text{eff}} \nabla T_{\text{f}}) \tag{4}$$

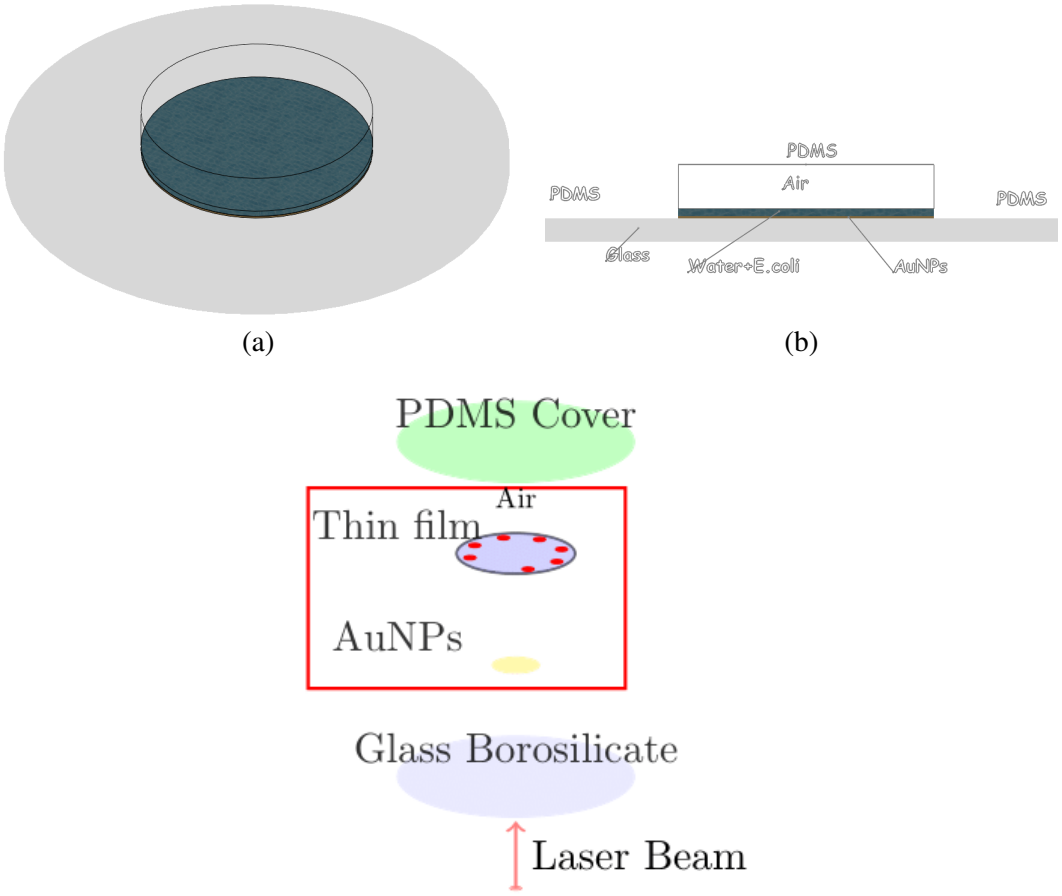

(a) (b)

(c)

Fig. 1 (a). 3D presentation of the microfluidic devise, (b). cross middle section, (c). Scheme of the experiment

- Solid region
  Conduction equation

$$\rho_{s_i} \frac{\partial (Cp_{s_i} T_{s_i})}{\partial t} = \nabla \cdot (k_{s_i} \nabla T_{s_i}) \tag{5}$$

3.2.2 Effective Thermal Properties : The simulation incorporates effective thermal properties in the all governing equations to faithfully represent the presence of E. coli in the thin water film. Effective thermal proprieties of mixture (water-bacteria) [26]

$$\rho_{\text{eff}} = (1-\phi)\rho_{\text{w}} + \phi\rho_{\text{bac}} \tag{6}$$

$$(\rho Cp)_{\text{eff}} = (1-\phi)(\rho Cp)_{\text{w}} + \phi(\rho Cp)_{\text{bac}} \tag{7}$$

$$(\rho\beta)_{\text{eff}} = (1-\phi)(\rho\beta)_{\text{w}} + \phi(\rho\beta)_{\text{bac}} \tag{8}$$

Effective dynamic viscosity with Brinkman model [27]:

$$\mu_{\text{eff}} = \frac{\mu_{\text{w}}}{(1-\phi)^{2.5}} \tag{9}$$

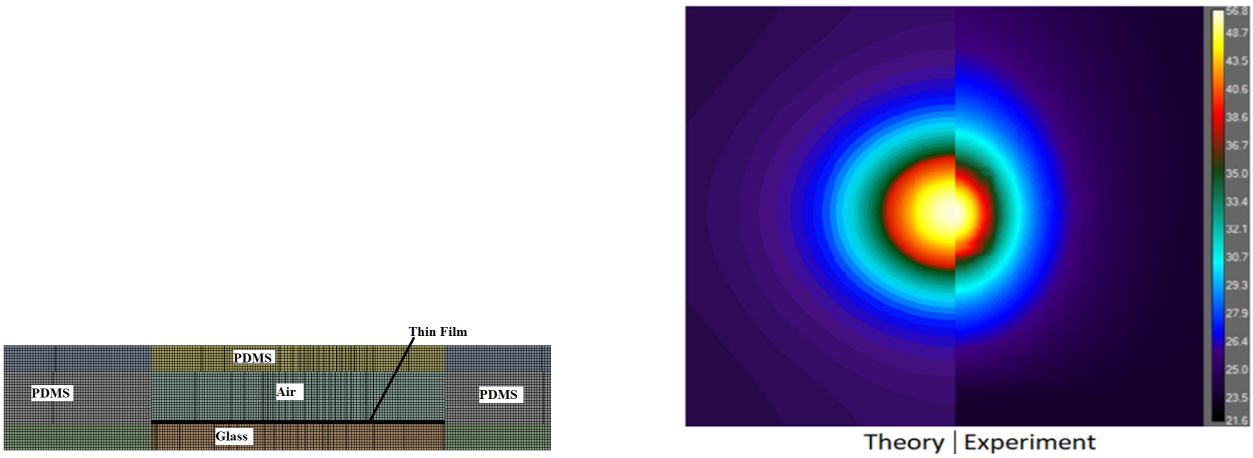

(a) (b)

Fig. 2 (a) Mesh cross-section , (b)Temperature filed : Experiment vs Numeric

Effective thermal conductivity with Lewis and Nielsen model :

$$k_{\text{eff}} = \frac{1 + S(\frac{k_{\text{bac}}/k_{\text{w}} - 1}{k_{\text{bac}}/k_{\text{w}} + S})\phi}{1 - (\frac{k_{\text{bac}}/k_{\text{w}} - 1}{k_{\text{bac}}/k_{\text{w}} + S})(1 + (\frac{1-\phi_{\text{m}}}{\phi_{\text{m}}^2})\phi)\phi} \tag{10}$$

3.3 Bacteria Deactivation and Kinetics

3.3.1 UDS : In conjunction with the standard conservation equations (mass, momentum, and energy) defined by eqs. (2) to (4), a pivotal "User Defined Scalar" (UDS) equation is introduced to intricately capture the kinetics of E. coli deactivation, thereby imparting a nuanced layer to the simulation. This additional equation takes the form:

$$\frac{\partial \rho N}{\partial t} + \frac{\partial}{\partial x_{\text{i}}}(\rho u_{\text{i}} N - \Gamma \frac{\partial N}{\partial x_{\text{i}}}) = S_{\text{N}} \tag{11}$$

- $\frac{\partial \rho N}{\partial t}$: This term represents the change rate of scalar quantity N with respect to time (t). It reflects the way in which E. coli concentration evolves over time in response to various factors (temperature rise).
- $\frac{\partial}{\partial x_{\text{i}}}(\rho u_{\text{i}} N - \Gamma \frac{\partial N}{\partial x_{\text{i}}})$: This term involves spatial derivatives and represents the advection and diffusion of the scalar N. It takes into account how the concentration is transported by fluid flow $\rho u_{\text{i}} N$ and diffused $\Gamma \frac{\partial N}{\partial x_{\text{i}}}$ in the spatial domain.

  - ρ is the density of the fluid. - u_{i} is the velocity component in the i-th direction. - Γ is the diffusivity, which controls the diffusion of N.
- S_{N}: This term represents any source or sink of the scalar N. In our context, it represents temperature-increasing influences during the irradiation process.

3.3.2 Skin Term: The UDS equation includes a skin term based on a first-order kinetic model [11, 12], reflecting the rate of thermal deactivation:

$$\frac{dN}{dt} = -KN \tag{12}$$

3.3.3 Arrhenius Equation: The decay coefficient (K) follows the Arrhenius equation, considering temperature-dependent parameters [11, 12]:

$$K = A \cdot exp(\frac{-Ea}{R \cdot T}) \tag{13}$$

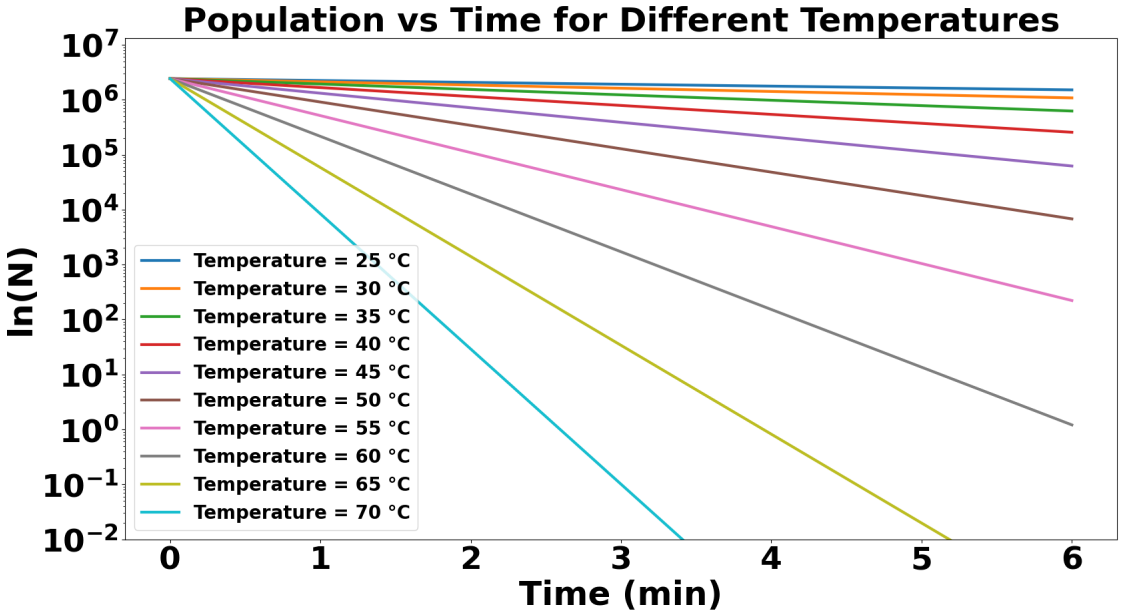

Fig. 3 Bacteria population decrease vs time for different temperature, $Ea = 80.9$ and $A = 19.5e10$

Here, A is the pre-exponential factor, Ea is the activation energy, R is the ideal gas constant, and T is the temperature. The Arrhenius equation provides a comprehensive means to model the exponential relationship between the rate constant and temperature, allowing for a nuanced representation of the temperature-dependent behaviour in the E. coli deactivation process.

3.4 Laser-Induced Heating:

Gold Nanoparticles: Well-established models simulate the laser-induced heating of gold nanoparticles [5, 13, 14], serving as localized heat sources in the microchamber, generating a controlled heat transfer based on the Lambert-Beer-Bouguer law:

$$q = \sigma_{\text{abs}_0} I_{\text{abs}} = \sigma_{\text{abs}_0}(1 - R_0) I_0 [1 - exp(-\sigma_{\text{abs}_0} \frac{l_{\text{gold}}}{\sqrt{(1 - \frac{sin(\alpha)}{n})}})] \tag{14}$$

The value of each parameter of above equation can be found in [13].

3.5 Numerical Implementation

3.5.1 Numerical Procedure and Mesh Generation The numerical simulation employed Ansys_FLUENT-23 R1 [24], a computational fluid dynamics commercial software. The Volume of Fluid (VOF) method and Continuous Surface Force (CSF) model were adopted. Convective terms in the momentum and energy equations were discretized using a second-order upwind scheme. Velocity–pressure coupling utilized the SIMPLE algorithm, with pressure interpolation performed using the PRESTO scheme. A first-order non-iterative scheme with a variable time step was used for the transient term integration until $t = 190$ s, where the maximum chamber temperature stabilized. The time step was set at 0.0002, and convergence criteria ensured residuals for all equations were below 10^{-8}. A uniform cubic grid with swelling near the bottom of the chamber, with refinement at the thin film of water, was generated (see Fig. 2 (a)).

3.5.2 UDFs Implementation

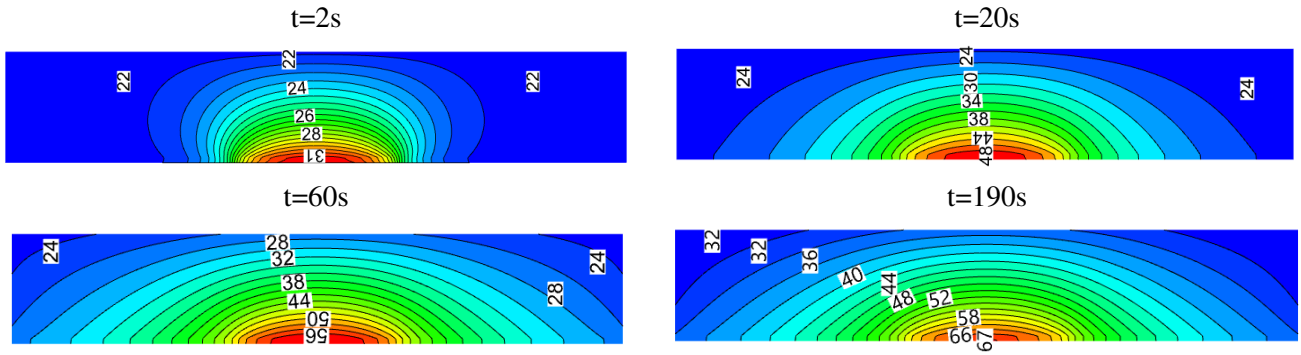

Fig. 4 Isotherms in the middle cross section of the chamber at different moment of simulation

- Effective Thermal Properties
  - The `DEFINE_PROPERTY` macro defined the thin film of water's effective thermal properties, considering bacterial presence via eqs. (8) to (10).
  - The `DEFINE_SPECIFIC_HEAT` macro determined the effective specific heat using eq. (7).
- Heat Generation Rate
  - The `DEFINE_PROFILE` macro integrated heat generation equation 14. A specified 3x3 mm^2 surface on the chamber bottom was irradiated, and this UDF applied only to that surface.
- Skin Term - The `DEFINE_SOURCE` macro defined a User-Defined Function (UDF) for calculating the skin term of the UDS equation.
  - A first-order kinetic model determined the rate of thermal deactivation ($\frac{dN}{dt}$) using the Arrhenius equation with parameters (A, Ea, R, T).
  - The UDF initialized and updated bacterial concentration (N) at each time step, representing temperature's influence on the deactivation process. Monitoring variables stored current concentration, previous concentration, and decay rate.

3.5.3 Validation with Benchmark Case: The numerical model underwent validation against experimental results (see Fig. 2 (b)). Temperature field results demonstrated both qualitative and quantitative agreement between experimental and numerical outcomes.

3.6 Arrhenius equation parameters

To determine the parameters of the Arrhenius equation for bacterial inactivation, systematically follow the steps below. Start by setting the initial bacterial population (N_0) at 10^6 and a constant time (t) of 3 minutes. Perform 5 tests at different temperatures (e.g. 25, 35, 45, 55, 65, 75°C), calculating the number of surviving bacteria (N) at each temperature after 3 minutes. Apply first-order kinetics to find the decay coefficient $k = -\frac{1}{t} ln\left(\frac{N}{N_0}\right)$. Then plot a curve relating $ln(k)$ to the inverse of temperature ($(1/T)$). Continue fitting the curve to these data using a linearized Arrhenius equation, obtaining the slope and y-intercept. The slope corresponds to $(-\frac{E_a}{R})$, and the y-intercept corresponds to $\ln(A)$. Finally, calculate the activation energy (E_a) and pre-exponential factor (A) from these fitted parameters.

As expected and in line with previous studies of bacterial dynamics at constant temperatures, the figure 3 reveals interesting information about population behaviour after 6 minutes. At lower temperatures, the bacterial population shows a sustained and minimal change, in line with expectations. Conversely, at higher temperatures, a marked and rapid reduction in the bacterial population is observed, corresponding to the expected impact of high temperatures on bacterial inactivation. This consistent pattern underlines the reliability of temperature as a critical factor influencing bacterial survival dynamics, confirming trends observed in previous studies.

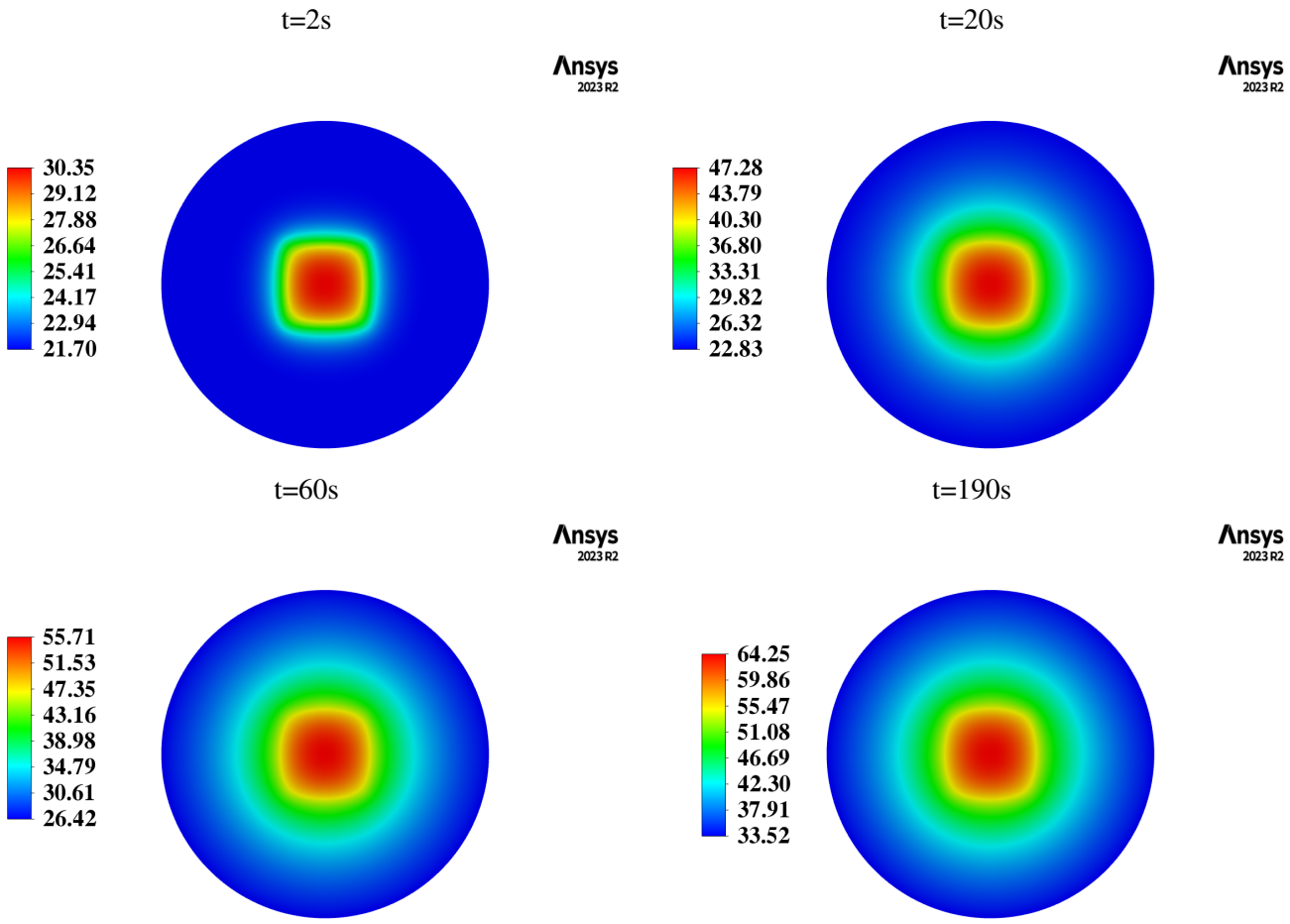

Fig. 5 Temperature filed in the interface water-air at different simulation time

4. RESULTS

In our examination of heat transfer dynamics inside the microfluidic chamber, the spatial distribution of temperature evolution provides valuable insights into thermal behavior during the irradiation process (see Dig.4). Notably, at the start of the experiment (t=2s), a sparse distribution of isotherm lines is observed, reflecting an incipient stage in the absorption of energy by the gold nanoparticles. The maximum temperature recorded at this stage is T=31°C, indicating a relatively low thermal intensity as the system responds to the external stimulus.

As the irradiation process progresses, the heat-generating effect intensifies, as shown by the increasing density of isotherm lines inside the chamber. This signifies a more dynamic state in response to sustained energy input, leading to higher temperature gradients. The most remarkable observation is the exponential increase in maximum chamber temperature between the start of the simulation (t=0s) and 60s of irradiation. During this critical phase, the system rapidly absorbs energy, resulting in a substantial temperature increase of 34°C. The highest temperatures are concentrated in the center of the chamber base, underlining the localized heating effect. After this initial phase, from t=60s to the end of the simulation at t=190s, a more gradual increase in temperature is observed. This suggests a transition to a more stabilized state, where the system reaches equilibrium and the rate of temperature increase becomes smaller. A continuous temperature rise of a moderate 11°C during this period indicates a controlled and sustained distribution of heat in the microfluidic environment.

The temperature contour at the air-water film interface plays a key role in understanding the complex heat transfer mechanisms operating in the microfluidic device.

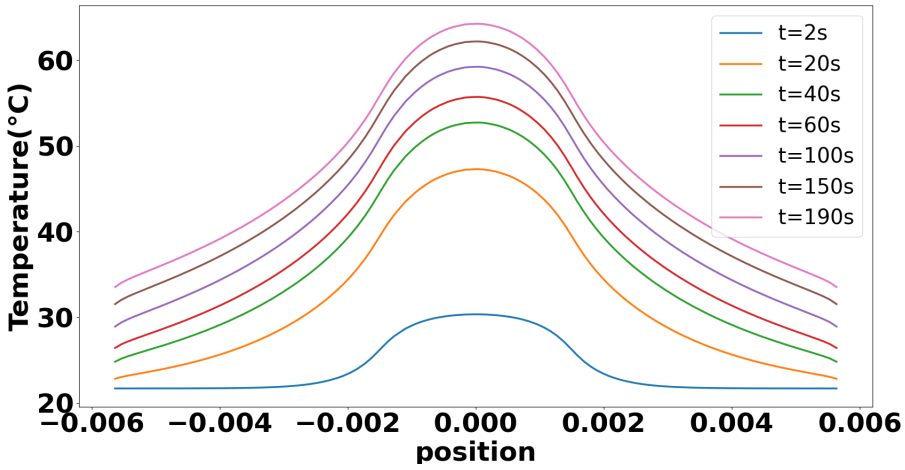

(a)

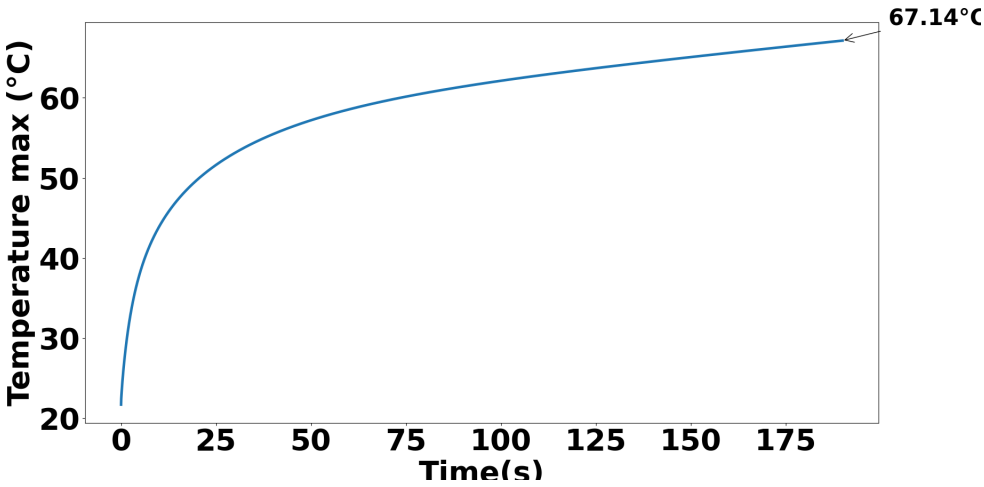

(b)

Fig. 6 (a) Temperature variation at middle line of the interface surface water-air for different time of simulation , (b) maximum temperature vs irradiation time

When we examine the temperature dynamics at this interface, a key parameter is the temperature gradient, i.e. the rate at which the temperature changes between the interface and the bottom of the chamber. This gradient is essential for assessing the efficiency of heat transfer processes within the microfluidic system.

By comparing the maximum temperatures at different times between the bottom of the chamber (Fig. 4) and the air-water interface (Fig. 5), a notable trend emerges. The temperature gradient within the thin film of water undergoes a perceptible increase over time. This observation implies that the temperature difference between the air-water interface and the bottom of the chamber becomes more pronounced as the simulation progresses. The intensification of the temperature gradient suggests a change in heat transfer mechanisms. At the start of the simulation, heat transfer is mainly by conduction. However, over time, the increase in temperature gradient indicates a transition to a quasi-convective regime. This change can be attributed to the cumulative effects of laser irradiation on the gold nanoparticles and their subsequent interaction with the surrounding medium.

The temperature profile along the air-water interface, as illustrated in Fig. 6a, gives a nuanced insight into the evolution of heat transfer dynamics inside the microfluidic chamber. The asymmetrical distribution, with

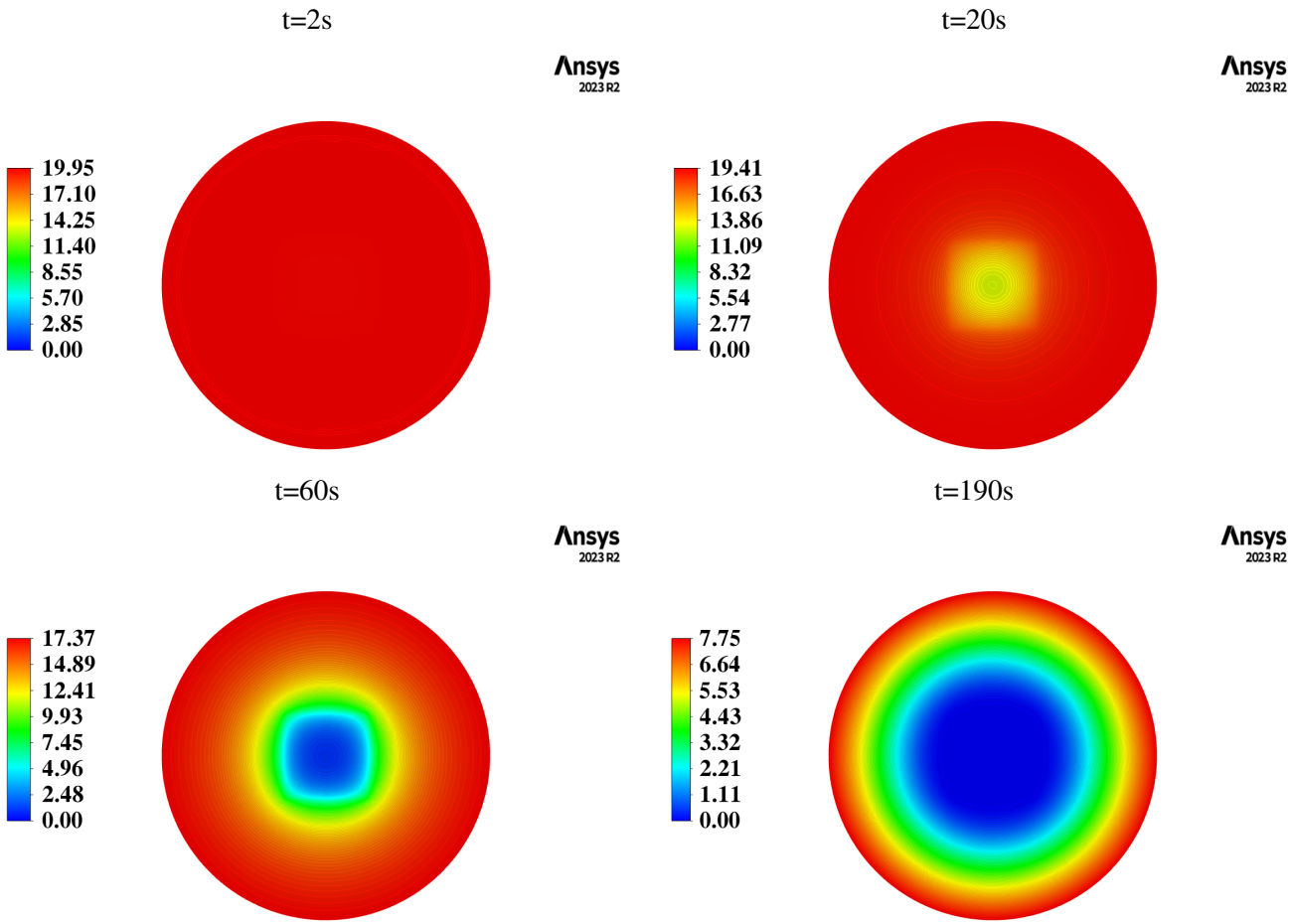

Fig. 7 Bacteria concentration in each cell of chamber bottom for different time of the process

temperatures peaking in the center and decreasing towards the sides, signifies the localized impact of laser irradiation and heat generation from the gold nanoparticles. The initial rapid rise in temperature, observed for each specific time interval of the simulation, is followed by a reduction in the distance between the curves. This reduction suggests a decrease in the rate of temperature increase over time, indicating a dynamic change in system response. It implies that as the simulation progresses, the temperature increase becomes more gradual, highlighting a transition in the heat dynamics inside the microfluidic chamber. Simultaneously, figure 6b highlights the relationship between maximum temperature variation in the fluidic chamber and time. The rapid rise in temperature during laser initiation is attributed to heat generation from the gold nanoparticles exceeding the dissipation rate, leading to an accumulation of thermal energy. Over time, dissipation mechanisms take hold, progressively increasing the rate of heat dissipation. The transition from an initially rapid increase to a more gradual one signifies a crucial shift, with dissipation mechanisms gaining in importance to balance heat production.

How the temperature field correlates with bacterial inactivation is clarified by analyzing the bacterial concentration on the bottom surface of the chamber. Fig. 7 shows the concentration of the UDS variable, which represents the bacterial population on the bottom surface at different times during the simulation. At the start of the simulation (t=2s), the entire surface is saturated with viable bacteria, which is the baseline condition.

As time passes and temperatures rise, a perceptible reduction in bacterial concentration becomes evident. Notably, the central region of the surface shows the greatest decline, reflecting the prevalence of inactive bacteria due to high localized temperatures. This spatial variation is represented visually in Fig. 7, highlighting the dynamic response of bacterial populations to changing thermal conditions. Fig. 8 also illustrates the temporal

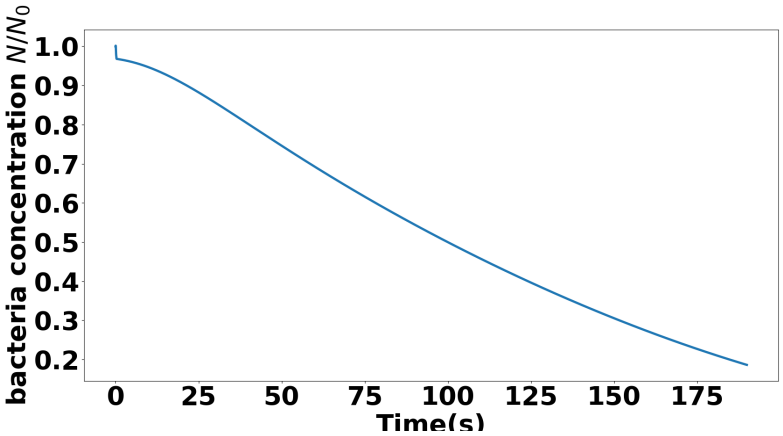

Fig. 8 Bacteria concentration vs irradiation time

evolution of bacterial concentration during the irradiation process. A rapid and abrupt reduction in bacterial concentration is observed at the start of the simulation (from 0s to 10s), indicating the immediate impact of the heat treatment. After that, the reduction in bacterial concentration follows a quasi-linear pattern as time elapses. It is remarkable that over 80% of the bacterial population is inactivated during the 190-second experiment, underlining the substantial effectiveness of the irradiation process in bacterial inactivation.

5. CONCLUSION:

In conclusion, our study presented a comprehensive numerical simulation aimed at clarifying the dynamics of thermal inactivation of E. coli bacteria in a microfluidic system. The system, composed of air and a thin film of water containing bacteria, integrates the principles of thermal physics, microbiology and computational fluid dynamics (CFD). Our model is validated against experimental results by means of thermal field observations, attesting to its fidelity. This work highlighted successful implementation of CFD coupling, namely VOF (Volume of Fluid Model), in conjunction with a first-order reaction model to explain bacterial population reduction and microorganism inactivation kinetics. A user-defined function (UDF) was developed, using an implicit integration method that calculates bacterial inactivation at each iteration and time step while taking into account existing temperature conditions. This implicit integration method improves the accuracy of the representation of the reduction in bacterial concentration over time. In addition, our CFD-based simulations demonstrate the remarkable effectiveness of laser irradiation of gold nanoparticles in inactivating bacteria.

ACKNOWLEDGMENTS

The work was supported by the National Science Centre, Poland, under research project “Shape and displacement optimization of gold nanorods in the killing chamber in order to photothermoablation processes”, no UMO-2021/43/D/ST8/02504. Computations were carried out using the computers of Centre of Informatics Tricity Academic Supercomputer & Network (CI TASK).

REFERENCES

[1] Taddese, Rahwa, et al. ”Production of inactivated gram-positive and gram-negative species with preserved cellular morphology and integrity.” Journal of Microbiological Methods 184 (2021): 106208.

[2] Espinosa, Maria Fernanda, et al. ”Systematic review and meta-analysis of time-temperature pathogen inactivation.” International Journal of Hygiene and Environmental Health 230 (2020): 113595.

[3] Mocan L, Tabaran FA, Mocan T, Pop T, Mosteanu O, Agoston-Coldea L, Matea CT, Gonciar D, Zdrehus C, Iancu C. Laser thermal ablation of multidrug-resistant bacteria using functionalized gold nanoparticles. Int J Nanomedicine. 2017 Mar 23;12:2255-2263. doi: 10.2147/IJN.S124778. PMID: 28356741; PMCID: PMC5367598.

[4] Govindaraju, Saravanan, et al. "Ultraviolet light and laser irradiation enhances the antibacterial activity of glucosamine-functionalized gold nanoparticles." International journal of nanomedicine 10.sup1 (2015): 67-78.

[5] Zaccagnini, Federica, et al. "White light thermoplasmonic activated gold nanorod arrays enable the photo-thermal disinfection of medical tools from bacterial contamination." Journal of Materials Chemistry B (2023).

[6] Petronella F., et al. "Label-free and reusable antibody-functionalized gold nanorod arrays for the rapid detection of Escherichia coli cells in a water dispersion." Environmental Science: Nano 9.9 (2022) 3343-3360.

[7] Tatsuno, Ichiro, et al. "Mechanism of transient photothermal inactivation of bacteria using a wavelength-tunable nanosecond pulsed laser." Scientific Reports 11.1 (2021): 22310.

[8] Spinks, Anthony T., et al. "Thermal inactivation of water-borne pathogenic and indicator bacteria at sub-boiling temperatures." Water research 40.6 (2006): 1326-1332.

[9] Cerf, O., K. R. Davey, and A. K. Sadoudi. "Thermal inactivation of bacteria—a new predictive model for the combined effect of three environmental factors: temperature, pH and water activity." Food Research International 29.3-4 (1996): 219-226.

[10] Park, Hyeon Woo, and Won Byong Yoon. "Computational fluid dynamics (CFD) modelling and application for sterilization of foods: A review." Processes 6.6 (2018): 62.

[11] Abu-Farah, L., and N. Germann. "Simulations of thermal phase changes and bacterial inactivation in a superheated steam dishwasher." Physics of Fluids 34.8 (2022).

[12] Ghani, AG Abdul, et al. "An investigation of deactivation of bacteria in a canned liquid food during sterilization using computational fluid dynamics (CFD)." Journal of food engineering 42.4 (1999): 207-214.

[13] Radomski, Piotr, et al. "Computational fluid dynamics simulation of heat transfer from densely packed gold nanoparticles to isotropic media." Archives of Thermodynamics (2021): 87-113.

[14] Radomski, Piotr, et al. "Heat Transfer of the Multicolor-Laser-Sources-Irradiated Nanoparticles in Reference to Thermal Processes." (2023).

[15] Park, Hyeon Woo, and Won Byong Yoon. "A quantitative microbiological exposure assessment model for Bacillus cereus in pasteurized rice cakes using computational fluid dynamics and Monte Carlo simulation." Food Research International 125 (2019): 108562.

[16] Xiong, R., et al. "A mathematical model for bacterial inactivation." International journal of food microbiology 46.1 (1999): 45-55.

[17] Ghani, A. G., M. M. Farid, and X. D. Chen. "Analysis of thermal sterilization of liquid food in cans and pouches using CFD." New Zealand Food Journal 30.6 (2000): 25-30.

[18] Feurhuber, Manuel, et al. "CFD simulation of the inactivation of Geobacillus stearothermophilus on dental handpieces." International Journal of Heat and Mass Transfer 144 (2019): 118649.

[19] Feurhuber, Manuel, et al. "Prediction of the fluid flow, heat transfer and inactivation of microorganism at medical devices in modern steam sterilizers using computational fluid dynamics." Applied Thermal Engineering 127 (2017): 1391-1403.

[20] Khatri, Shilpa, and Anna-Karin Tornberg. "A numerical method for two phase flows with insoluble surfactants." Computers & fluids 49.1 (2011): 150-165.

[21] Balachandran, S. H. U. A. I. B., et al. "Verification of Volume-of-Fluid (VOF) simulation for thin liquid film applications." 2009 3rd international conference on energy and environment (ICEE). IEEE, 2009.

[22] Qin, Ning, et al. "Numerical Study on Single Flowing Liquid and Supercritical CO2 Drop in Microchannel: Thin Film, Flow Fields, and Interfacial Profile." Inventions 3.2 (2018): 35.

[23] Mehdaoui, H., Abderrahmane, H. A., Bouda, F. N., Koulali, A., & Hamani, S. (2021). 2D numerical simulation of tear film dynamics: Effects of shear-thinning properties. European Journal of Mechanics-B/Fluids, 90, 128-136.

[24] ANSYS Inc. (2021). ANSYS Fluent (v2021 R1) [Computer software]. ANSYS Inc.

[25] Ziółkowski P., Badur J.: A theoretical, numerical and experimental verification of the Reynolds thermal transpiration law. International Journal of Numerical Methods for Heat & Fluid Flow, vol: 28(1); (2018): 64-80; DOI 10.1108/HFF-10-2016-0412.

[26] Koulali, Aimad, et al. "Comparative study on effects of thermal gradient direction on heat exchange between a pure fluid and a nanofluid: Employing finite volume method." Coatings 11.12 (2021): 1481.

[27] Brinkman, Hendrik C. "The viscosity of concentrated suspensions and solutions." The Journal of chemical physics 20.4 (1952): 571-571.